Room-Temperature Ferromagnetic $Ga_{1-x}Mn_xAs$ ($x \leq 0.05$) Nanowires: Dependence of Electronic Structures and Magnetic Properties on Mn Content

Han Sung Kim, Yong Jae Cho, Kang Jun Kong, Chang Hyun Kim, Gyeong Bok Chung, and Jeunghee Park*

Department of Chemistry, Korea University, Jochiwon 339-700, Korea

Jae-Young Kim

Pohang Accelerator Laboratory, POSTECH, Pohang 790-784, Korea

Jungbum Yoon, Myung-Hwa Jung,† and Younghun Jo

Quantum Material Research Team, Korea Basic Science Institute, Daejeon 305-333, Korea

Bongsoo Kim

Department of Chemistry, KAIST, Daejeon 305-701, Korea

Jae-Pyoung Ahn

Advanced Analysis Center, Korea Institute of Science and Technology, Seoul 136-791, Korea

Received December 11, 2008. Revised Manuscript Received January 21, 2009

$Ga_{1-x}Mn_xAs$ nanowires were synthesized with finely controlled Mn contents ($x = 0$, 0.01, 0.02, 0.03, and 0.05) by the vapor transport method. They consisted of single-crystalline GaAs nanocrystals (avg. diameter = 60 nm) grown along the [111] direction. The Mn doping decreases the lattice constant, most significantly at $x \approx 0.03$. X-ray photoelectron spectroscopy revealed that as the Mn content increases, the binding energy of Ga 2p shifts to a higher energy, which can be correlated with the hybridization between the Mn^{2+} ions and the holes. X-ray absorption spectroscopy and X-ray magnetic circular dichroism confirmed that the Mn^{2+} ions substitute into the tetrahedrally coordinated Ga sites and that the magnetic moment is maximized at $x = 0.03$, where the lattice constant is minimized and the binding energy of Ga 2p is maximized. The magnetization measurement revealed that all of these nanowires exhibited room-temperature ferromagnetic behavior, which is also observed most significantly for $x \approx 0.03$.

1. Introduction

Diluted magnetic semiconductors (DMSs), in which the host cations are randomly substituted by magnetic ions, have attracted a considerable amount of attention because of their excellent potential as key materials for spintronic devices.[1−3] The demonstration of the unique phenomena associated with DMSs, such as the field-effect control of their ferromagnetism, efficient spin injection to produce circularly polarized light, and spin-dependent resonant tunneling, has opened up a rich and various landscape for technological innovation in magnetoelectronics. As one of the most important ferromagnetic DMSs, Mn-doped GaAs ($Ga_{1-x}Mn_xAs$) has been extensively studied for more than two decades.[4−16] The spin 5/2 Mn (Mn^{2+}) ions at the regular sites of the zinc blende lattice of the GaAs host act as acceptors, thus providing both

* Corresponding author. E-mail: parkjh@korea.ac.kr.
† Present address: Department of Physics, Sogang University, Seoul 121-742, Korea.

(1) (a) Ohno, H. *Science* **1998**, *281*, 951. (b) Ohno, Y.; Young, D. K.; Beschoten, B.; Matsukura, F.; Ohno, H.; Awschalom, D. D. *Nature* **1999**, *402*, 790. (c) Ohno, H.; Chiba, D.; Matsukura, F.; Omiya, T.; Abe, E.; Dietl, T.; Ohno, Y.; Ohtani, K. *Nature* **2000**, *408*, 944.
(2) Fiederling, R.; Keim, M.; Reuscher, G.; Ossau, W.; Schmidt, G.; Waag, A.; Molenkamp, L. W. *Nature* **1999**, *402*, 787.
(3) Wolf, S. A.; Awschalom, D. D.; Buhrman, R. A.; Daughton, J. M.; von Molnár, S.; Roukes, M. L.; Chtchelkanova, A. Y.; Treger, D. M. *Science* **2001**, *294*, 1488.
(4) Ohno, H.; Shen, A.; Matsukura, F.; Oiwa, A.; Endo, A.; Katsumoto, S.; Iye, Y. *Appl. Phys. Lett.* **1996**, *69*, 363.
(5) Oiwa, A.; Katsumoto, S.; Endo, A.; Hirasawa, M.; Iye, Y.; Ohno, H.; Matsukura, F.; Shen, A.; Sugawara, Y. *Solid State Commun.* **1997**, *103*, 209.
(6) Dietl, T.; Ohno, H.; Matsukura, F.; Cibert, J.; Ferrand, D. *Science* **2000**, *287*, 1019.
(7) Sanvito, S.; Ordejón, P.; Hill, N. A. *Phys. Rev. B* **2001**, *63*, 165206.
(8) Erwin, S. C.; Petukhov, A. G. *Phys. Rev. Lett.* **2002**, *89*, 227201.
(9) Jungwirth, T.; Konig, J.; Sinova, J.; Kučera, J.; MacDonald, H. *Phys. Rev. B* **2002**, *66*, 012402.
(10) (a) Mahadevan, P.; Zunger, A. *Phys. Rev. B* **2003**, *68*, 075202. (b) Mahadevan, P.; Zunger, A.; Sarma, D. D. *Phys. Rev. Lett.* **2004**, *93*, 177201.
(11) Bergqvist, L.; Korzhavyi, P. A.; Sanyal, B.; Mirbt, S.; Abrikosov, I. A.; Nordström, L.; Smirnova, A. E.; Mohn, P.; Svedlindh, P.; Eriksson, O. *Phys. Rev. B* **2003**, *67*, 205201.
(12) Krstajić, P. M.; Peeters, F. M.; Ivanov, V. A.; Fleurov, V.; Kikoin, K. *Phys. Rev. B* **2004**, *70*, 195215.
(13) Schulthess, T. C.; Temmerman, W. M.; Szotek, Z.; Butler, W. H.; Stocks, G. M. *Nat. Mater.* **2005**, *4*, 838.
(14) Kitchen, D.; Richardella, A.; Tang, J.-M.; Flatté, M. E.; Yazdani, A. *Nature* **2006**, *442*, 436.

10.1021/cm8033388 CCC: $40.75
Published on Web 03/02/2009

magnetic moments and itinerant holes which mediate the ferromagnetic order. Nowadays, their ferromagnetism is fairly well understood, thus allowing their Curie temperatures to be predicted. In this respect, Mn-doped GaAs is one of the best understood ferromagnetic materials. Dietl et al. predicted the Curie temperature (T_C) of 5% Mn-doped p-type GaAs ($Ga_{0.95}Mn_{0.05}As$) to be 120 K, by the Zener model description.[6] The quest to increase the T_C to room temperature has led to a thorough investigation of the material properties. Experimentally, it was reported that annealing ($\leq$200 °C) for a long time can lead to a significant improvement in its T_C, with values as high as 159 K being reported.[15] The magnetic properties were enhanced with a value of T_C = 250 K being reached, as it forms Mn-δ doping heterostructures.[16]

The majority of these studies on $Ga_{1-x}Mn_xAs$ focused on the bulk materials, but its integration into electronics will require very low dimensions in order to make real use of the advantages offered by the spins. The calculations predicted that the quantum confinement effect can even increase the magnetic properties in certain nanosize regimes.[17,18] Recently, intensive research activities have been directed toward one-dimensional (1D) nanostructures, which are considered to be building blocks for the fabrication of various nanoscale devices. In particular, well-defined single-crystalline nanowires enable us to scrutinize precisely the magnetic properties and electronic structures of DMSs depending on their crystal size and Mn doping levels. There have been a number of reports on the synthesis of Mn ($\leq$20%)-doped GaAs nanowires (NWs), showing a wide range of T_C values from 30 to 350 K.[19−24] In order to fully understand their magnetic properties, it is important to elucidate the electronic structures which are responsible for their magnetic properties. However, the correlations between their electronic structures and magnetization are far from being well understood. Furthermore, the fine control of Mn contents in the nanowire structure has not been reported yet.

Herein, we synthesized high-purity single-crystalline $Ga_{1-x}Mn_xAs$ NWs with controlled Mn contents, x = 0, 0.01, 0.02, 0.03, and 0.05, exhibiting room-temperature (T_C > 350 K) ferromagnetism, using a simple vapor transport method. The Mn content was controlled by using different evaporation temperatures of the Mn source ($MnCl_2$). Their lattice constants and electronic structures were first thoroughly investigated as a function of the Mn concentration by high-resolution X-ray diffraction (XRD), X-ray photoelectron spectroscopy (XPS), X-ray absorption spectroscopy (XAS), and X-ray magnetic circular dichroism (XMCD). We attempted to correlate the magnetization of these nanowires with their electronic structures.

2. Experimental Section

GaAs (99.999%, Aldrich) and $MnCl_2$ (99.99%, Aldrich) powders were placed separately in two quartz boats loaded inside a quartz tube reactor. A silicon substrate, on which a 3−5 nm thick Au film was deposited, was positioned at a distance of 10 cm away from the GaAs source. Argon gas was continuously flowed at a rate of 500 sccm during the synthesis. The temperatures of the Ga and Mn sources were set to 1000 and 800 °C, respectively, and that of the substrate was approximately 800−850 °C. The products were analyzed by scanning electron microscopy (SEM, Hitachi S-4700), field-emission transmission electron microscopy (TEM, FEI TECNAI G^2 200 kV), high-voltage TEM (HVEM, Jeol JEM ARM 1300S, 1.25 MV), and energy-dispersive X-ray fluorescence spectroscopy (EDX).

High-resolution XRD patterns were obtained using the 8C2 beam line of the Pohang Light Source (PLS) with monochromatic radiation (λ = 1.54520 Å). XPS (ESCALAB 250, VG Scientifics) using a photon energy of 1486.6 eV (Al Kα) was employed to investigate the electronic states. Synchrotron XPS measurements were also performed at the U7 beam line of the PLS. The XAS and XMCD measurements were carried out at the Pohang Light Source (PLS) elliptically polarized undulator beamline, 2A. The samples were introduced into an experimental chamber with a base pressure of 5×10^{-10} Torr. The spectra were collected in the total electron yield (TEY) mode. A 0.6 T electromagnet was used to switch the magnetization direction. The magnetization direction was flipped between the parallel (ρ+) and antiparallel (ρ-) directions with respect to the photon helicity vector for each data point. The degree of circular polarization (95%) of the incident light was taken into account in the spectra. The magnetic properties were studied using a superconducting quantum interference device (SQUID, Quantum Design) magnetometer.

3. Results and Discussion

3.1. Morphology and Composition. The growth mechanism of the nanowires follows the vapor−liquid−solid (VLS) mechanism, which makes use of the Au catalytic nanoparticles. The Mn content was controlled by adjusting the evaporation temperature of $MnCl_2$. Figure 1a shows the SEM micrograph of the high-density 2% Mn-doped GaAs ($Ga_{0.98}Mn_{0.02}As$) NWs grown on the substrates. The TEM image explicitly reveals their smooth surface and average diameter of 60 nm (Figure 1b). The Au catalytic-nanoparticles are frequently attached to the tips, providing evidence for the VLS growth mechanism. The lattice-resolved TEM

(15) Edmonds, K. W.; Bogusławski, P.; Wang, K. Y.; Campion, R. P.; Novikov, S. N.; Farley, N. R. S.; Gallagher, B. L.; Foxon, C. T.; Sawicki, M.; Dietl, T.; Buongiorno Nardelli, M.; Bernholc, J. *Phy. Rev. Lett.* **2004**, *92*, 037201.
(16) Nazumul, A. M.; Amemiya, T.; Shuto, Y.; Sugahara, S.; Tanaka, M. *Phy. Rev. Lett.* **2005**, *95*, 017201.
(17) Sapra, S.; Sarma, D. D.; Sanvito, S.; Hill, N. A. *Nano Lett.* **2002**, *2*, 605.
(18) Huang, X.; Makmal, A.; Chelikowsky, J. R.; Kronik, L. *Phys. Rev. Lett.* **2005**, *94*, 236801.
(19) (a) Martelli, F.; Rubini, S.; Piccin, M.; Bais, G.; Jabeen, F.; De Franceschi, S.; Grillo, V.; Carlino, E.; D'Acapito, F.; Boschrini, F.; Cabrini, S.; Lazzarino, M.; Businaro, L.; Romanato, F.; Franciosi, A. *Nano Lett.* **2006**, *6*, 2130. (b) Martelli, F.; Piccin, M.; Bais, G.; Jabeen, F.; Ambrosini, S.; Rubini, S.; Franciosi, A. *Nanotechnology* **2007**, *18*, 125603. (c) Rubini, S.; Piccin, M.; Bais, G.; Jabeen, F.; Martelli, F.; Franciosi, A. *J. Phys.: Conf. Ser.* **2007**, *61*, 992.
(20) (a) Wagner, K.; Neumaier, D.; Reinwald, M.; Wegscheider, W.; Weiss, D. *Phys. Rev. Lett.* **2006**, *97*, 056803. (b) Neumaier, D.; Wagner, K.; Geiβler, S.; Wurstbauer, U.; Sadowski, J.; Wegscheider, W.; Weiss, D. *Phys. Rev. Lett.* **2007**, *99*, 116803.
(21) Sheu, B. L.; Eid, K. F.; Maksimov, O.; Samarth, N.; Schiffer, P. *J. Appl. Phys.* **2006**, *99*, 08D501.
(22) Jeon, H. C.; Kang, T. W.; Kim, T. W.; Yu, Y.-J.; Jhe, W.; Song, S. A. *J. Appl. Phys.* **2007**, *101*, 023508.
(23) (a) Vila, L.; Giraud, R.; Thevenard, L.; Lemaître, A.; Pierre, F.; Dufouleur, J.; Mailly, D.; Barbara, B.; Faini, G. *Phys. Rev. Lett.* **2007**, *98*, 027204. (b) Giraud, R.; Vila, L.; Lemaître, A.; Faini, G. *Appl. Surf. Sci.* **2007**, *254*, 343.
(24) Sadowski, J.; Dłużewski, P.; Kret, S.; Janik, E.; Łusakowska, E.; Kanski, J.; Presz, A.; Terki, F.; Charar, S.; Tang, D. *Nano Lett.* **2007**, *7*, 2724.

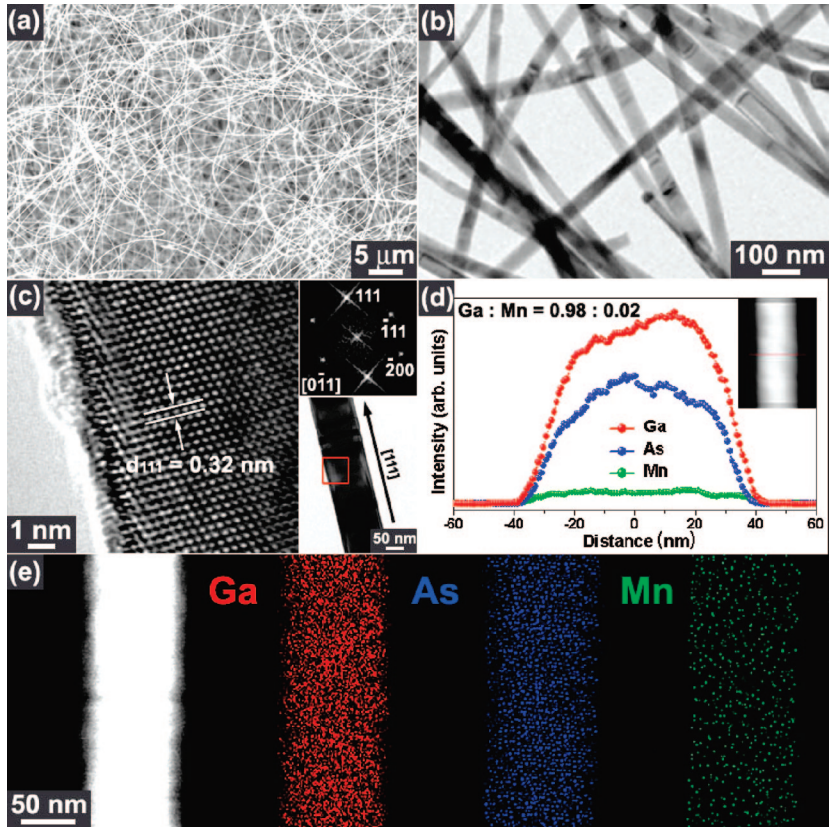

Figure 1. (a) SEM micrograph of high-density $Ga_{0.98}Mn_{0.02}As$ NWs, homogeneously grown on the substrate. (b) TEM image reveals that they have a straight morphology with a uniform diameter of 60 nm. (c) Lattice-resolved image of selected NW revealing its single-crystalline nature; the distance between the neighboring (111) planes is 3.2 Å. The TEM image and corresponding FFT ED pattern confirm the[11] growth direction (insets). (d) EDX line-scan profile of Ga, As, and Mn for a selected $Ga_{0.98}Mn_{0.02}As$ NW, whose STEM image is shown in the inset. (e) STEM image (left) and EDX elemental mapping reveals the homogeneous composition of Ga, As, and Mn. The average Mn content is 0.05 ± 0.01.

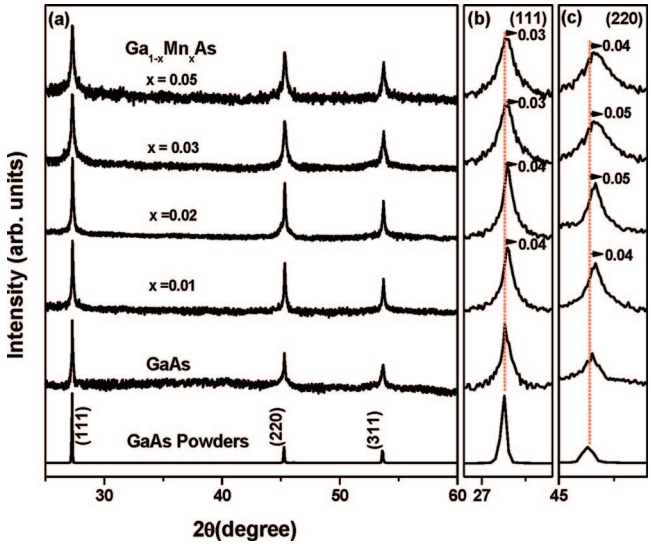

Figure 2. (a) Full-range XRD patterns taken from the $Ga_{1-x}Mn_xAs$ ($x = 0$, 0.01, 0.02, 0.03, and 0.05) NWs, and the magnified scaled (b) (111) and (c) (220) peaks.

image and corresponding fast Fourier-transform electron diffraction (FFT ED) pattern of a selected nanowire reveal that it is composed of single-crystalline zinc blende structured GaAs (Figure 1c and two insets). It shows a spacing between neighboring (111) planes of ca. 3.2 Å, which is consistent with that of the bulk materials ($a = 5.654$; JCPDS Card no. 80−0016). The FFT ED pattern generated from the inversion of the TEM image using DigitalMicrograph GMS1.4 software (Gatan Inc.), at the [0$\bar{1}$1] zone axis, confirms that it has the [111] growth direction. The EDX line-scanning analysis indicates the Mn content (x = [Mn]/([Ga]+[Mn])) of the individual nanowire to be about $x = 0.02 \pm 0.01$, with a homogeneous distribution being observed along the cross-section, as shown in Figure 1d. The inset corresponds to its high-angle annular dark field (HAADF) scanning TEM (STEM) image. The STEM image and its EDX mapping for a selected $Ga_{0.95}Mn_{0.05}As$ NW are shown in Figure 1e. The Mn element is distributed homogenously over the whole nanowire with an average Mn content of 0.05 ± 0.01. The average value was obtained from the EDX measurement of 4−8 nanowires. Further atomic-resolved TEM images and corresponding FFT ED pattern were measured along the single $Ga_{0.95}Mn_{0.05}As$ NW, showing the single-crystalline GaAs phase with no cluster formation (see the Supporting Information, Figure S1).

The $Ga_{1-x}Mn_xAs$ NW samples were selectively synthesized with controlled Mn contents, i.e., 0, 0.01 ± 0.01, 0.02 ± 0.01, 0.03 ± 0.01, and 0.05 ± 0.01, all having a similar morphology to that of the $Ga_{0.98}Mn_{0.02}As$ NWs. The EDX data of an individual nanowire of each of these five samples are shown in the Supporting Information, Figure S2. The XPS spectrum of the $Ga_{1-x}Mn_xAs$ NWs is shown in the Supporting Information, Figure S3. The Mn content was obtained using the integration of the Ga and Mn 2p peaks and is consistent with the average value obtained from the EDX data.

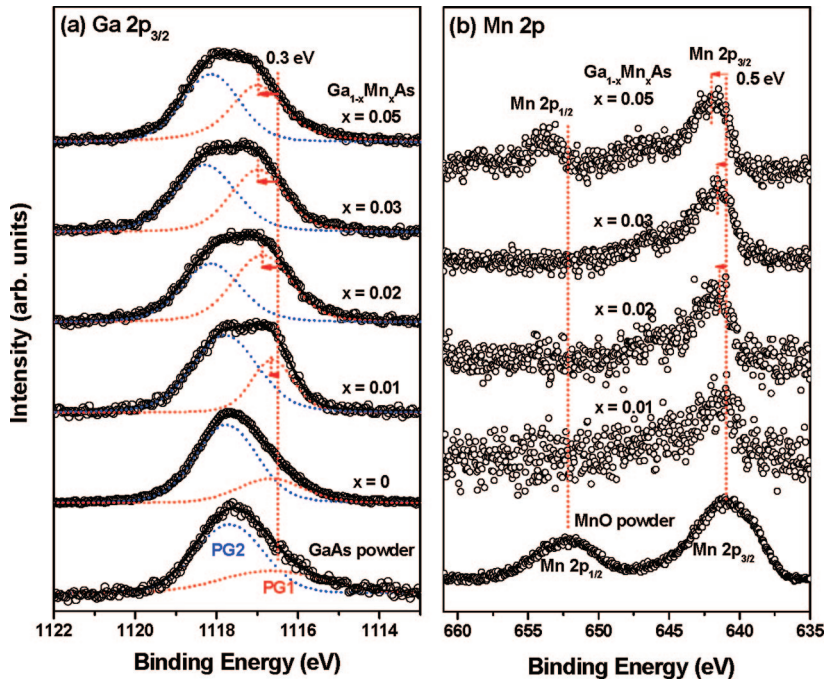

Figure 3. Fine-scanned XPS spectra of (a) Ga $2p_{3/2}$ of the $Ga_{1-x}Mn_xAs$ ($x = 0$, 0.01, 0.02, 0.03, and 0.05) NWs, and (b) Mn $2p_{3/2}$ and $2p_{1/2}$ of the MnO powder and $Ga_{1-x}Mn_xAs$ ($x = 0.01$, 0.02, 0.03, and 0.05) NWs.

3.2. XRD: Expansion of Lattice Constants by Mn Doping. The high-resolution XRD patterns of the undoped GaAs NWs and $Ga_{1-x}Mn_xAs$ NWs are displayed in Figure 2a. The peaks of the GaAs NWs exactly match those of zinc blende GaAs ($a = 5.654$; JCPDS Card no. 80−0016). All of the GaAs NW samples have a highly crystalline nature without the presence of other phases. Panels b and c in Figure 2 display the magnified (111) and (220) peaks, respectively. The peak position shifts to a higher angle, most significantly when the Mn content is 0.02−0.03. The maximum shifts, $\Delta(2\theta)$, of the (111) and (220) peaks are 0.04 and 0.05°, respectively. Their peak width becomes broader as the Mn concentration increases.

If the Ga^{3+} ions ($r_{Ga} = 0.61$ Å at the tetrahedral sites) were substituted with the larger radius Mn^{2+} ions ($r_{Mn} = 0.80$ Å), the lattice constant would expand because of the difference in the ionic radius. In the present study, however, the lattice constant decreases initially until $x = 0.02-0.03$, and then slightly increase, while still remaining smaller than that of the undoped NWs. The decrease of the lattice constants reaches to 0.14% for the (111) plane, and 0.11% and (110) plane. This decreasing-to-increasing behavior of the lattice constant is consistent with the results obtained for $Ga_{1-x}Mn_xN$ ($x \leq 0.05$) NWs, which showed an increase in their lattice constant above $x = 0.03$.[25] This reduced lattice constant can be ascribed to the hybridization between the Mn dopants and host defects (holes), as discussed in section 3.3. This minimized lattice constant is also well correlated with the maximized magnetic moments, as discussed in sections 3.4 and 3.5.

3.3. Fine-Scanned XPS: Electronic Structure of Ga and Mn Atoms. The XPS survey scans show the Ga, As, and Mn peaks (see the Supporting Information, Figure S3). The feature of the fine-scanned Ga 2p peaks was strongly dependent on the Mn content. Figure 3a shows the fine-scanned Ga $2p_{3/2}$ peak. The peak of the $Ga_{1-x}Mn_xAs$ NWs is broader in width and more asymmetric, as compared to that of the undoped one. Furthermore, as the Mn content increases, the peak position shifts to the higher energy region. The peak can be deconvoluted into two bands at ~1117 (PG1) and ~1118 (PG2) eV. The peak position, full-width at half-maximum (fwhm), and area % of the deconvoluted bands are listed in Table 1. The binding energy of the Ga atoms bonded to the As atoms would be expected to appear at a lower energy compared to that of the Ga atoms bonded to dangling bonds or defects (usually bonded to more electronegative O atoms). Therefore, the PG1 and PG2 bands can be assigned to the Ga−As and Ga−O bonding structures, respectively. As the Mn dopes, the area % of the PC2 band tends to decrease, suggesting that the substitution of the Ga sites reduces the oxide layers. As the Mn content increases, the peak position of the PG1 band shifts to the higher energy region; 0.2 eV $x = 0.02$; 0.3 eV for $x = 0.03$ and 0.05. The

Table 1. Peak Positions (eV), FWHMs (eV), and Area % Values of the Deconvoluted Bands from the XPS Ga $2p_{3/2}$ Peaks, and Peak Positions of the Mn $2p_{3/2}$ Peaks, for the $Ga_{1-x}Mn_xAs$ ($x = 0$, 0.01, 0.02, 0.03, and 0.05) NWs, GaAs Powder, and MnO Powder

	Ga $2p_{3/2}$						
	PG1 (Ga−As)			PG2 (Ga−O)			Mn $2p_{3/2}$
x_{Mn}	position (eV)	fwhm (eV)	area %	position (eV)	fwhm (eV)	area %	position (eV)
powder[a]	1116.7	3.0	33	1117.7	2.0	67	640.8
0	1116.7	1.9	25	1117.8	1.8	75	
0.01	1116.7	1.7	36	1117.8	2.0	64	641.2
0.02	1116.9	1.7	53	1118.1	1.7	47	641.5
0.03	1117.0	1.6	45	1118.3	1.8	55	641.6
0.05	1117.0	1.6	49	1118.1	1.7	51	641.7

[a] GaAs powder for Ga $2p_{3/2}$ peak, and MnO powder for Mn $2p_{3/2}$ peak.

(25) Hwang, S. O.; Kim, H. S.; Park, S.-H.; Park, J.; Bae, S. Y.; Kim, B.; Park, J. Y.; Lee, G. *J. Phys. Chem. C* **2008**, *112*, 2934.

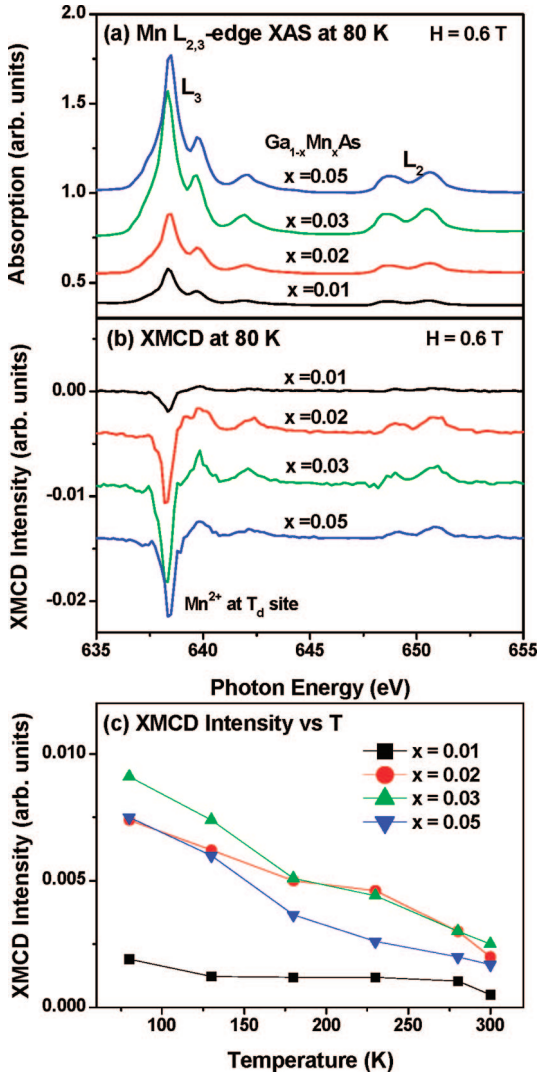

Figure 4. (a) XAS and (b) XMCD spectra of Mn $L_{2,3}$ edge, measured for the $Ga_{1-x}Mn_xAs$ ($x = 0.01$, 0.02, 0.03, and 0.05) NWs under $H = 0.6$ T, at 80 K. (c) Temperature dependence ($T = 80$, 130, 180, 230, 280, and 300 K) of the XMCD intensity for $x = 0.01$, 0.02, 0.03, and 0.05.

PG2 band also show a tendency to shift to a higher-energy; 0.3 eV for $x = 0.02$; 0.5 eV for $x = 0.03$; 0.3 eV for $x = 0.05$. The peak shows the highest energy shift for $x = 0.03$.

Figure 3b corresponds to the finely scanned Mn $2p_{3/2}$ and $2p_{1/2}$ peaks of the Mn-doped GaAs NWs. The peak of the MnO powders is also displayed for comparison. All NWs exhibit the higher binding energy than that of the Mn(II)−O bonding structure. Furthermore, as the Mn content increases to $x = 0.05$, the position of Mn $2p_{3/2}$ peak continuously shift toward the higher energy region, with a maximum shift of 0.5 eV being observed. This peak shift toward the higher-energy region is attributed to the hybridized bonding structures, as discussed below.

The present Mn-doped GaAs NWs exhibit ferromagnetic properties, which will be discussed below (section 3.5). For the room-temperature ferromagnetic Co-doped ZnO nanoparticles reported by Xu and co-workers, there was a strong correlation between the XPS peak position and the saturation magnetic moment.[26] The shift of the Zn 2p core-level toward the higher energy region was maximized for $x = 0.056$, showing the same trend as the saturation magnetic moment. For Mn-doped ZnO, GaN, and Ge NWs, our group also observed the maximum higher-energy shift of the XPS peaks at certain Mn content, and the remarkable correlation with the magnetic moment.[25,27,28] We suggested that the hybridization between the Mn dopant and the holes would lead to a higher binding energy shift. As regards the origin of the ferromagnetism of the Mn-doped GaAs, in p-type GaAs, there exists an acceptor's hole transfer process onto Mn^{2+} to form Mn^{3+}, as described by the relation $Mn^{2+} + h^+$ (acceptor) $\rightarrow Mn^{3+}$. This hybridization is the pivotal feature determining the value of T_C in theoretical models describing DMS ferromagnetism.[29,30] The higher-energy shift of the Mn 2p peaks can be also an indication of such hybridization. As the Mn content increases from $x = 0.03$ to $x = 0.05$, the Ga peak does not continue to move toward a higher energy, a behavior which can be explained by the reduced hybridization. The XRD data shows a minimum value of the lattice constant at $x = 0.02-0.03$, which would be directly related to the fact that the maximum hybridization takes place at this point.

3.4. XAS and XMCD. To further investigate the electronic structure of the Mn ions, we performed XAS and XMCD ($\Delta\rho = \rho^+ - \rho^-$) measurements at the Mn $L_{2,3}$ edges. Panels a and b in Figure 4 show the Mn $L_{2,3}$ edge XAS and XMCD spectra of the $Ga_{1-x}Mn_xAs$ ($x = 0.01$, 0.02, 0.03, and 0.05) NWs, respectively, measured at 80 K. The spectra, which result from the Mn $2p \rightarrow 3d$ dipole transition, are divided roughly into the L_3 ($2p_{3/2}$) and L_2 ($2p_{1/2}$) regions. Figure 4c displays the intensity of the XMCD L_3 peak as a function of temperature ($T = 80$, 130, 180, 230, 280, and 300 K), for the $Ga_{1-x}Mn_xAs$ NWs, showing a monotonous decrease with increasing temperature, and a maximum for $x = 0.03$.

The peak features and positions of the XAS spectra suggest that the doped Mn atoms are in an ionic state, not in a metallic state such as metallic Mn clusters. The negative signal of the XMCD L_3 peak can be clearly observed, indicating the contribution of Mn^{2+} at the tetrahedral (T_d) sites, substituting for the Ga ions in GaAs, which is consistent with the results obtained for Mn-doped GaAs films.[31,32] These Mn^{2+} ions would be responsible for the hybridization (discussed in section 3.3), which results in the ferromagnetism of the GaAs NWs. The magnetic moments are not zero, even at room temperature. As the Mn content increases, the intensity of the XMCD peaks increases continuously up to $x = 0.03$, and then decreases when $x = 0.05$. The temperature-dependence of the intensity shows no sudden decrease, suggesting that $T_C > 300$ K. The magnetic moment

(26) Wang, X.; Xu, J.; Zhang, B.; Yu, H.; Wang, J.; Zhang, X.; Yu, J.; Li, Q. *Adv. Mater.* **2006**, *18*, 2476.
(27) Kang, Y. J.; Kim, D. S.; Lee, S. H.; Park, J.; Chang, J.; Moon, J. Y.; Lee, G.; Yoon, J.; Jo, Y.; Jung, M.-H. *J. Phys. Chem. C* **2007**, *111*, 14956.
(28) Cho, Y. J.; Kim, C. H.; Kim, H. S.; Lee, W. S.; Park, S.-H.; Park, J.; Bae, S. Y.; Kim, B.; Lee, H.; Kim, J.-Y. *Chem. Mater.* **2008**, *20*, 4694.
(29) Kittilstved, K. R.; Liu, W. K.; Gamelin, D. R. *Nat. Mater.* **2006**, *5*, 2914.
(30) Radovanovic, P. V.; Barrelet, C. J.; Gradečak, S.; Qian, F.; Lieber, C. M. *Nano Lett.* **2005**, *5*, 1407.
(31) Keavney, D. J.; Wu, D.; Freeland, J. W.; Johnston-Halperin, E.; Awschalom, D. D.; Shi, J. *Phy. Rev. Lett.* **2003**, *91*, 187203.
(32) Edmonds, K. W.; van der Laan, G.; Freeman, A. A.; Farley, N. R. S.; Johal, T. K.; Campion, R. P.; Foxon, C. T.; Gallagher, B. L.; Arenholtz, E. *Phy. Rev. Lett.* **2006**, *96*, 117207.

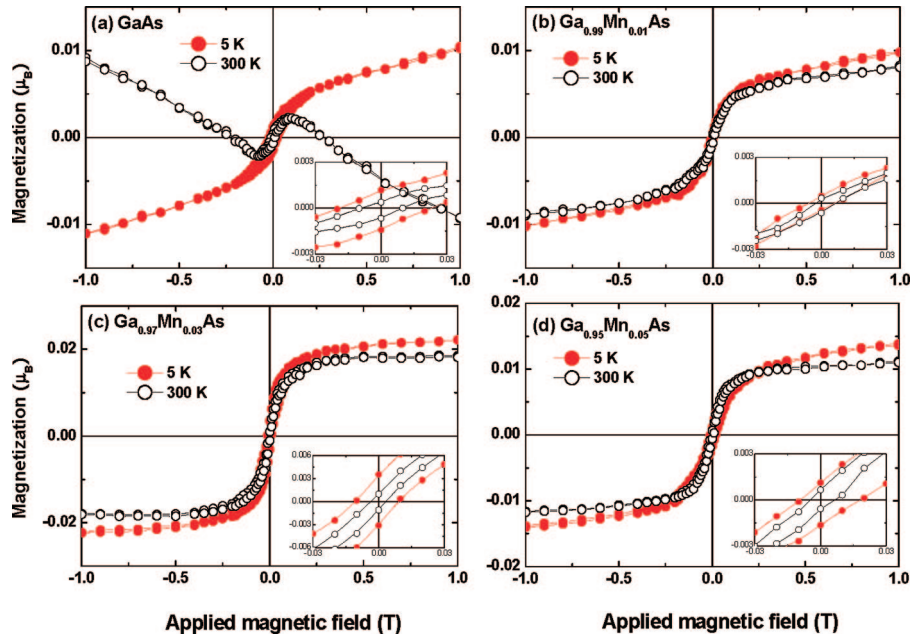

Figure 5. Field-dependent magnetic moment ($M-H$) curves for (a) GaAs, (b) $Ga_{0.99}Mn_{0.01}As$, (c) $Ga_{0.97}Mn_{0.03}As$, (d) $Ga_{0.95}Mn_{0.05}As$ NWs, measured at 5 and 300 K. The inset represents the magnified $M-H$ curve in the vicinity of $H = 0$, showing the hysteresis.

is highest for $x = 0.03$, at all temperatures, which is well-correlated with the magnetization measured by SQUID, as shown in section 3.5.

3.5. Magnetization. The magnetic moment (M) versus magnetic field (H) curves at 5 and 300 K were measured by the SQUID magnetometer. The nanowires were separated from the substrates. All of the samples exhibit ferromagnetic hysteresis behavior with a diamagnetic and/or paramagnetic background signal (not deducted in the figures). Figure 5a corresponds to the field-dependent $M-H$ curve of the undoped GaAs NWs. Hysteresis occurs with a saturation field of 0.1 T at both temperatures. The saturated magnetization is estimated to be 0.005 μ_B at 5 K. The inset displays the curve in the vicinity of $H = 0$, indicating that the coercive field (H_C) is 200 Oe and the remanence (M_r) is 0.0015 μ_B at 5 K. Therefore, the existence of ferromagnetism at 5 and 300 K is clearly proven by the coercivity and remanence, and relatively low saturation field, suggesting that the T_C value is at least 300 K. The field-cooled (FC) and zero-field-cooled (ZFC) magnetization versus temperature (M_{FC} and M_{ZFC} vs T) curves with $H = 500$ Oe are displayed in the Supporting Information, Figure S4, indicating that $T_C > 350$ K.

Figure 5b–d displays the $M-H$ curves of the $Ga_{0.99}Mn_{0.01}As$, $Ga_{0.97}Mn_{0.03}As$, and $Ga_{0.95}Mn_{0.05}As$ NWs, respectively, consistently showing hysteresis at 5 and 300 K. The saturated magnetizations of these NWs are estimated to be about 0.005, 0.02, and 0.01 μ_B at 5 K, respectively. The hysteresis curves show that $M_r = 0.0007$, 0.004, and 0.0015 μ_B and $H_C = 75$, 110, and 100 Oe, for $x = 0.01$, 0.03, and 0.05, respectively, at 5 K (inset). As the Mn content increases from $x = 0.01$ to $x = 0.03$, the magnetization increases by a factor of ~5. As it increases further to $x = 0.05$, the M_r decreases by a factor of ~2. This result indicates that the magnetization reaches a maximum for $x = 0.03$. The M_{FC} and M_{ZFC} vs T curves indicate that $T_C > 350$ K (see the Supporting Information, Figure S4).

The ferromagnetic behaviors of the undoped GaAs NWs are quite surprising. Recently, the size-dependent ferromagnetism of Ge nanoparticles (deposited on polystyrene or Si substrates) has been reported.[33] Our research group also observed room-temperature ferromagnetic properties for Ge NWs, and suggested that this originated from the existence of uncompensated spins and surface anisotropy, because of the high surface/volume ratio.[28] Further investigation is necessary to clearly explain the ferromagnetic properties of the GaAs NWs. We are currently conducting calculations and experiments to examine of the catalyst effect on the magnetic properties.

The magnetic moment of the $Ga_{1-x}Mn_xAs$ NWs overwhelms that of the undoped GaAs NWs, and reaches a maximum with $x = 0.03$. This result is consistent with the XAS and XMCD data showing that the Mn substitution with $x = 0.03$ leads to the greatest increase in the magnetic moment of the Mn^{2+} ions. These results suggest that the magnetization of the $Ga_{1-x}Mn_xAs$ NWs reaches a maximum when $x = 0.03$. This result is consistent with the XPS data showing that the Mn substitution with $x = 0.03$ is most effective in increasing the dopant-acceptor hybridization. A reduced level of magnetization at a higher concentration ($x > 4-5\%$) was observed from the film, which is consistent with the present result.[5,34]

4. Conclusion

Single-crystalline $Ga_{1-x}Mn_xAs$ ($x = 0$, 0.01, 0.02, 0.03, and 0.05) NWs were grown by the vapor transport method, using the evaporation of $GaAs/MnCl_2$. They all consist of single-crystalline zinc blende GaAs crystals grown uniformly

(33) (a) Liou, Y.; Su, P. W.; Shen, Y. L. *Appl. Phys. Lett.* **2007**, *90*, 182508. (b) Liou, Y.; Lee, M. S.; You, K. L. *Appl. Phys. Lett.* **2007**, *91*, 082505.
(34) Ishiwata, Y.; Wanatabe, M.; Eguchi, R.; Takeuchi, T.; Harada, Y.; Chainani, A.; Shin, S.; Hayashi, T.; Hashimoto, Y.; Katsumoto, S.; Iye, Y. *Phy. Rev. B* **2002**, *65*, 233201.

with the [111] direction, regardless of the level of Mn doping. The EDX data reveal that the Mn dopes homogeneously over the entire nanowires. We investigated their electronic structures and magnetic properties by XRD, XPS, XAS, XMCD, and MPMS. The XRD data reveal that the lattice constant decreases with increasing Mn doping level, most significantly at $x = 0.02-0.03$. The positions of the XPS Ga and Mn 2p peaks shift to the higher energy region when x is increased. We explained the higher-energy peak shift in terms of the hybridization between the Mn^{2+} ions and holes, which was suggested to be a crucial feature in determining the ferromagnetism. The XAS and XMCD data reveal that the Mn^{2+} ions are dominantly present at the T_d sites, substituting for the Ga ions. The magnetization measurement using SQUID reveals that they all exhibit ferromagnetic behaviors at room temperature, even the undoped NWs. The $Ga_{1-x}Mn_xAs$ NWs exhibit a much larger magnetic moment than the undoped NWs, and consistently exhibit a maximum value at $x = 0.03$, which is well correlated with the minimum value of the lattice constant and maximum values of the binding energy of Ga at this Mn content. We conclude that the most effective ferromagnetic nanowires are formed when the Mn content is ~0.03, under our experimental conditions.

Acknowledgment. This work was supported by KRF grants (KRF-2008-314-C00175), KOSEF (R01-2008-000-10825-0; M1080300121808), and MKE under the ITRC support program supervised by the IITA (IITA-2008-C1090-0804-0013). The SEM, TEM, HVEM, XRD, and XPS measurements were performed at the KBSI in Seoul, Daejeon, Taegu, Pusan, respectively. J.-P.A. is grateful to KIST for its financial support. The experiments at the PLS were partially supported by MOST and POSTECH.

Supporting Information Available: HRTEM images of $Ga_{0.95}Mn_{0.05}As$ NWs; EDX data, full-range XPS data for $Ga_{1-x}Mn_xAs$ ($x = 0.01$, 0.02, 0.03, and 0.05) NWs; MPMS data (PDF). This material is available free of charge via the Internet at http://pubs.acs.org.

CM8033388